Chemical Science Review and Letters ISSN 2278-6783

Research Article

Structural and Optical Properties of Cu Doped ZnO Nanoparticles

D. Guruvammal[1*], S. Selvaraj[1] and S. Meenakshi Sundar[2]

[1]PG and Research Department of Physics, The M.D.T. Hindu College, Tirunelveli-627 010, M.S. University, Tirunelveli, Tamilnadu, India
[2]PG and Research Department of Physics, Sri Paramakalyani College, Alwarkurichi-627 412, M.S. University, Tirunelveli, Tamilnadu, India

Abstract

In this paper, different characterization techniques are employed to study the effects of copper doping on the structural and optical properties of zinc oxide (ZnO) nanoparticles synthesized by solvothermal method using domestic microwave oven. The X-Ray Diffraction (XRD) pattern indicates that the synthesized samples have a single phase wurtzite hexagonal structure of ZnO. The particle size calculated using Debye Scherrer's formula is also confirmed by Transmission Electron Microscope (TEM) studies. Scanning Electron Microscope (SEM) studies confirm uniform distribution of the samples and the elements present in the samples have been recorded by Electron Diffraction X-Ray (EDX) spectroscopy. The functional group of the samples has been confirmed by Fourier Transform Infra-Red (FTIR) analysis. UV-Visible (UV-Vis) spectrum shows a red shift in the absorption edge due to the incorporation of Cu^{2+} ions into ZnO lattice. A weak ultraviolet peak related to near band edge emission and a prominent peak corresponding to defect related visible emission are seen in the Photoluminescence (PL) spectra.

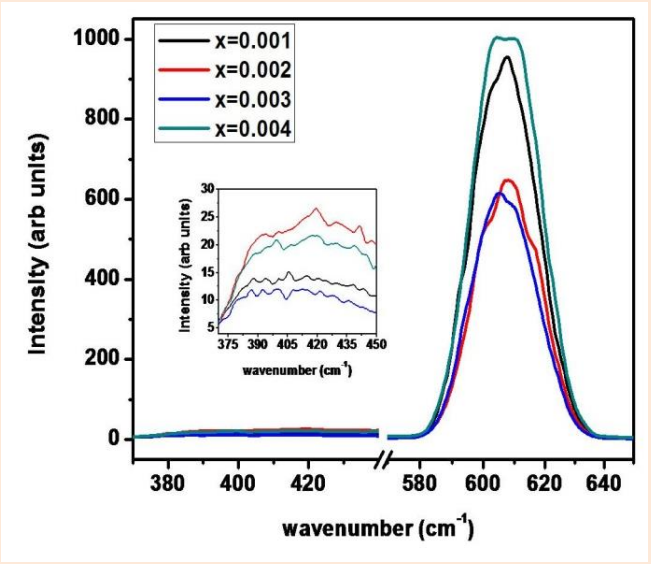

***Correspondence**
Author: D. Guruvammal
Email: gurudurai216@gmail.com

Keywords: ZnO Nanoparticles, Cu^{2+} doping, SEM & EDX, TEM, PL

Introduction

Transition metal (TM) doped semiconductor nanoparticles have been studied due to their promising fluorescence properties for technological applications [1]. ZnO is a unique material in II-VI semiconductor with wide band gap 3.37 eV, large exciton binding energy 60 meV. Doped ZnO is of considerable significance for its use in industry as information storage materials, fluorescence lamps, control panel displays, plasma display panels, field effect transistor [2-6], gas sensors [7], solar cells [8], varistors [9], light emitting devices [10], photocatalyst [11], antibacterial agent [12], cancer treatment [13], antireflecting coatings piezoelectric devices, surface acoustic wave propagator[14, 15] and photonic materials [16]. Theoretical and experimental studies showed that ZnO doped with appropriate TM are diluted magnetic semiconductors (DMS) [17] which have potential applications in spintronics [18]. The most commonly used metallic dopants in ZnO based systems are Al, Co, Cu, Ga, Sn etc [19-23]. Among them Cu is important because, (i) it can change the microstructure and the optical properties of the ZnO system [21], (ii) it has many physical and chemical properties that are similar to those of Zn and (iii) it is a prominent luminescence activator, which can modify the luminescence of ZnO crystals by creating localized impurity levels [24].

Different methods such as thermal decomposition, thermolysis [25], chemical vapor deposition, sol-gel [26], spray pyrolysis, precipitation [27], vapour phase oxidation [28], thermal vapour transport, condensation [29], co-precipitation [30], hydrothermal [31], auto-combustion method [32], ball milling method [33] and so on are available

in literature to synthesize ZnO nanoparticles. In this paper, solvothermal method is used to synthesize Cu doped ZnO nanoparticles with four different concentrations as this method has several advantages such as short reaction time, small particles size, narrow size distribution and high purity [34-40]. Further, structural and optical properties of the synthesized samples are also studied.

Experimental procedure

Materials and Reagents

Analytical grade precursor materials such as zinc acetate dihydrate [$(CH_3CO_2)_2Zn.2H_2O$], copper (II) acetate monohydrate [$(CH_3CO_2)_2Cu.H_2O$)], urea [H_2NCONH_2] were used to synthesize copper doped ZnO nanoparticles by solvothermal method. Ethylene glycol [$CH_2OH.CH_2OH$] was used as a solvent. In this process, zinc acetate, copper acetate and urea in the proposed ratios were mixed well with ethylene glycol and the mixture was stirred well for 1 hour using a magnetic stirrer. The stirred solution in a bowl was placed in a domestic microwave oven at a temperature of 80°C. The solution was microwave treated until the solvent evaporated completely. Further, the substance deposited in the bowl was taken out and washed at least four times with double distilled water and acetone to remove unwanted water soluble compounds and organic compounds present in the samples [41]. The synthesized nanoparticles were filtered, dried in sun light for one week and annealed in muffle furnace at 350°C for 1 hour to improve the crystallinity of samples.

Characterization techniques

The crystalline nature and the phase purity of our samples were analyzed by X-Ray Diffraction (XRD) recorded on a PAnalytical model X' Pert PRO diffractometer using Cu-K_α radiation (1.5406 A°) operated at 40 KeV and 30 mA in the angle range from 10° to 80° with step size 0.01°. The morphology of the sample was studied by Scanning electron microscopy (SEM, Carl Zeiss EVO 18 model). The composition of the materials was estimated by energy dispersive X-ray spectroscopy (EDX) (Quantax 200 with X – flash Bruker). The crystal size and morphology have been studied by transmission electron microscope (TEM) using Philips CM 200 with a point resolution of 2.4 A° and operating voltage 20 kV - 200 kV. The presence of chemical bonding in Ni doped ZnO nanoparticles was studied by Fourier Transform InfraRed (FTIR) spectrometer (Model: Perkin Elmer, Make: Spectrum RX1) in the range of 4000 - 400 cm^{-1} by the KBr pellet method. Optical absorbance measurements were carried out using UV-Visible spectrophotometer (Model: Lambda 35, Make: Perkin Elmer) in the wavelength ranges from 190 - 1100 nm to determine the optical band gap, while the Photoluminescence (PL) studies were carried out between the wavelengths ranges from 330 - 750 nm using luminescence spectrophotometer (Model: LS 35, Make: Perkin-Elmer). All measurements were performed at room temperature.

Results and Discussion

Structural Properties

Powder XRD studies

Figure 1a shows the XRD patterns of Cu doped ZnO ($Zn_{1-x}Cu_xO$, where x=0.001 to 0.004) powder samples annealed at 350°C. All the diffraction peaks correspond to (100), (002), (101), (102), (110), (103), (200), (112), (201), (004) and (202) crystal planes showing hexagonal structure of pure ZnO. The diffraction angles of the peaks matched very well with standard JCPDS card no. 89-0510 [42]. No additional peaks corresponding to any secondary phases such as CuO, Cu_2O or Cu clusters could be observed from the XRD patterns. The average crystallite size D_{hkl} using Debye - Scherrer's formula, the micro strain ε, bond length L and volume of unit cell V of the samples [43] can be calculated as $D_{hkl}=0.9\lambda/\beta\cos\theta$; $V=0.866*a^2*c$; $L = \sqrt{\frac{a^2}{3} + (\frac{1}{2} - u)^2 * c^2}$; $\varepsilon = (\beta\cos\theta)/4$. Here $u = a^2/(3c^2) + 0.25$ and λ, β, θ, u, a, and c refer to wavelength of the X-rays (λ=1.5406 A°), full width half-maximum (FWHM), Bragg angle, parameter for wurtzite structure and lattice parameters respectively. The calculated values are listed in **Table 1**. The average crystallite size of Cu doped ZnO nanoparticles is found to be in the range of 11 - 25 nm. The change in lattice parameters clearly indicates the incorporation of Cu^{2+} ions into the ZnO lattice without disturbing the structure of ZnO. Varying peak position and lattice parameters reveal ionic size mismatch between Zn^{2+} (0.74 A°) and Cu^{2+} (0.73 A°) ions. The c/a parameter is found to be 1.6 which is close to the standard value of close packed hexagonal

structure. The bond length decreases as the content increases up to x=0.002 and then increases for the further increase of concentration. This variation in bond length may be due to the formation of Cu-O bonds in addition to Zn-O bonds in ZnO lattice. This Cu-O bond length is smaller than that of Zn-O. A small change of 2θ values for a prominent peak corresponding to 101 plane observed in Figure 1b may be due to size or micro strain or size and micro strain of nanoparticles [44]. Figure 1c shows the relation between particle size and micro strain with Cu concentration. From this figure, it is observed that the micro strain of Cu doped sample decreases and the size of the nanoparticles increases when Cu concentration is increased.

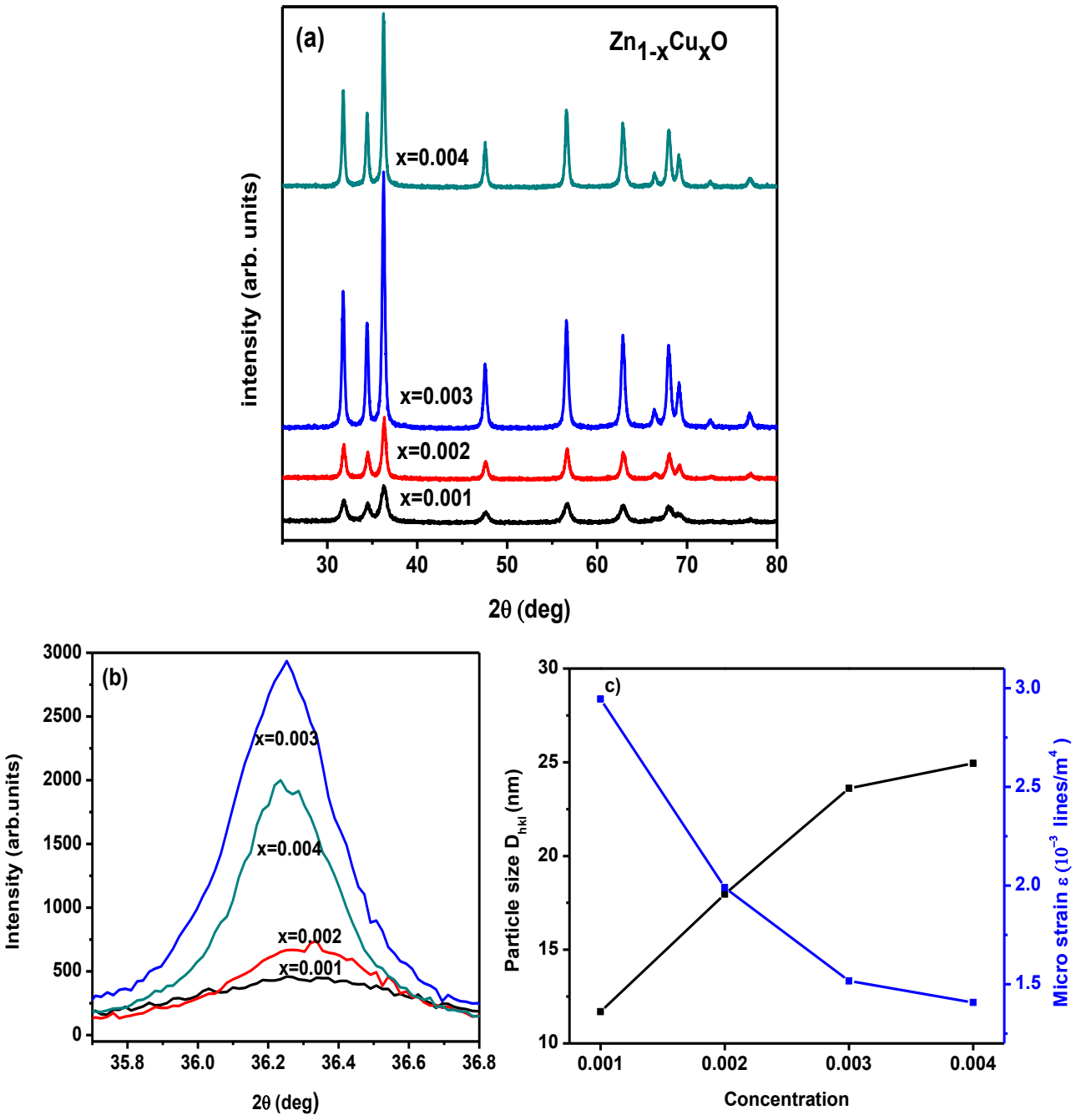

Figure 1 XRD patterns of (a) $Zn_{1-x}Cu_xO$ nanoparticles annealed at 350°C (b) Diffraction peak for 101 plane and (c) Relation between particle size, micro strain with Cu concentration

Table 1 Lattice parameter, Particle size, Volume of unit cell, Bond length and Micro strain of $Zn_{1-x}Cu_xO$ nanoparticles.

Copper concentration	Lattice parameters (A°)		c/a	Particle size D_{hkl} (nm)	Volume of unit cell V ($A°^3$)	Bond length L (nm)	Micro strain ε (10^{-3} lines/m^4)
	a=b	c					
x=0.001	3.2523	5.1977	1.5982	11.69	47.6113	1.9777	2.945
x=0.002	3.247	5.1968	1.6005	17.96	47.4480	1.9754	1.990
x=0.003	3.2482	5.2049	1.6024	23.61	47.5571	1.9769	1.516
x=0.004	3.2475	5.2041	1.6025	24.94	47.5293	1.9765	1.408

SEM & EDX studies

SEM image of the prepared $Zn_{0.999}Cu_{0.001}O$ nanoparticles is shown in **Figure 2a** and **Figure 2b**. The synthesized nanoparticles are observed to be homogeneous, dense and distributed uniformly over the surface. The recorded EDX spectrum of the sample is shown in Figure 2c. From this figure, the weight percentage of elements such as Cu, Zn and O present in the synthesized sample is obtained. This result confirms that the weight percentage of Cu in the prepared samples (0.08 %) is nearly equal to the stoichiometric weight percentage of Cu (0.1 %) taken for preparing the sample. The Cu^{2+} ions are replacing the Zn^{2+} ions in the ZnO lattice site. The oxygen signal at 0.52 KeV, zinc signals at 1.01 KeV and 8.66 KeV and the copper signal at 0.9 KeV and 8.02 KeV are observed.

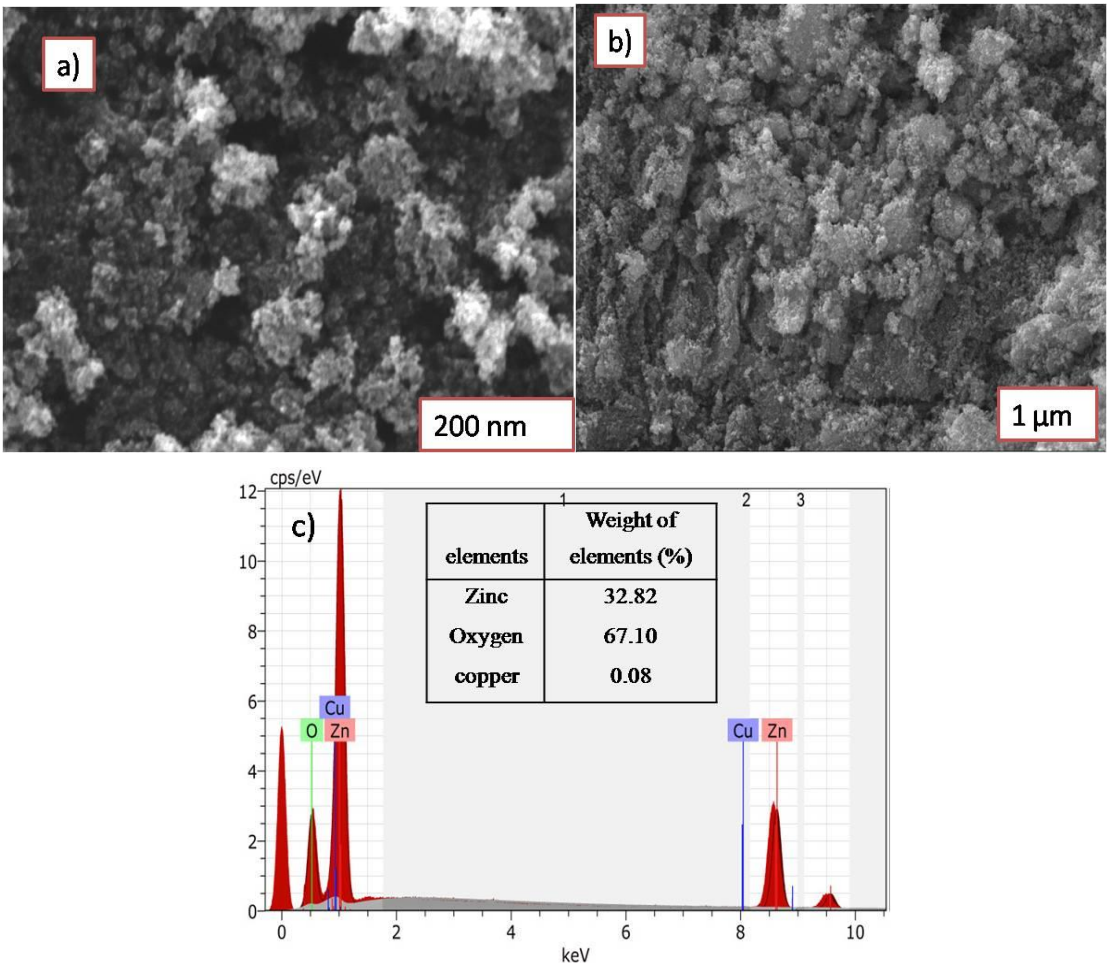

Figure 2 (a) and (b) SEM images of $Zn_{0.999}Cu_{0.001}O$ nanoparticles (c) EDX image of $Zn_{0.999}Cu_{0.001}O$ nanoparticles. Inset, shows the elemental composition of samples

TEM studies

The TEM image of $Zn_{0.999}Cu_{0.001}O$ nanoparticles is shown in **Figure 3a**. It is observed that Cu doped ZnO nanoparticles are nearly hexagonal in shape with uniform particle size distribution having diameter range from 18.36 - 22.34 nm and this result is in good agreement with the one obtained from XRD patterns.

The Selected Area Electron Diffraction pattern (SAED) of the sample is shown in Figure 3b and is indexed to the wurtzite ZnO structure for all planes and this result matches well with the XRD pattern of the samples. SAED pattern reveals that no additional rings were observed besides the diffraction rings of wurtzite structure of ZnO.

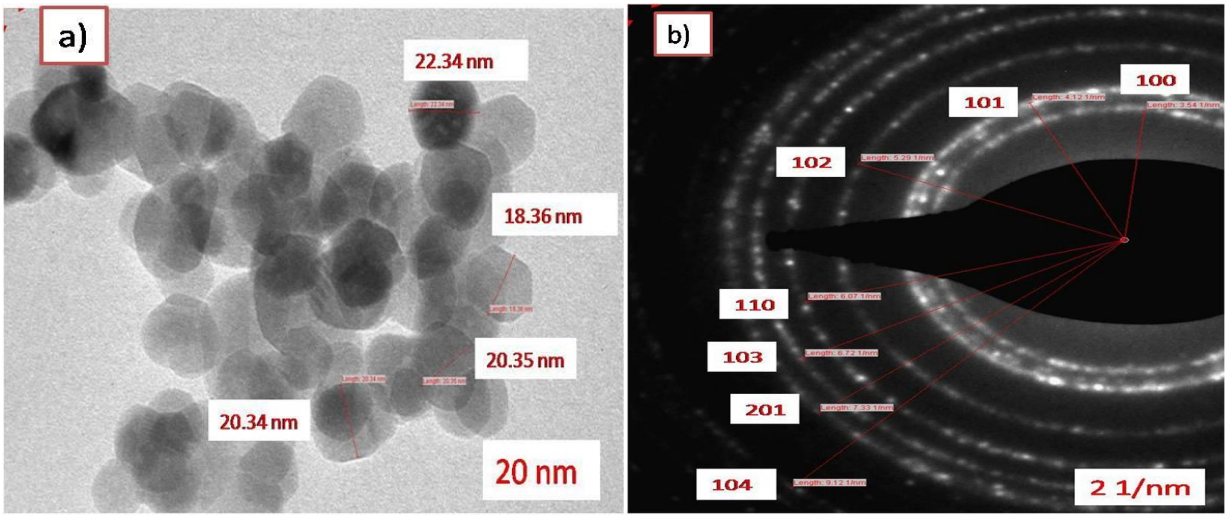

Figure 3(a) TEM image and **(b)** SAED patterns for $Zn_{0.999}Cu_{0.001}O$ nanoparticles

Optical Properties

FTIR studies

Figure 4 shows the FTIR spectra of Cu doped ZnO nanoparticles annealed at 350°C in the wave number range of 400 cm^{-1} – 4000 cm^{-1}. The peak observed at ~ 3429 cm^{-1} and 1598 cm^{-1} are attributed to O-H stretching vibration and H-O-H bending vibration respectively due to the existence of small amount of H_2O in the surface of ZnO [45]. A weak band observed at ~ 2921 cm^{-1} might be due to some residual organic compound present in the samples. A peak is observed at ~ 1392 cm^{-1} due to carbonyl group present on the surface of ZnO [46]. In general, the peak observed between 400 - 600 cm^{-1} is ascribed to metal-oxygen (M-O) i.e. Zn-O stretching vibration. The absorption band located around 550 cm^{-1} is because of the stretching vibration of ZnO [47].

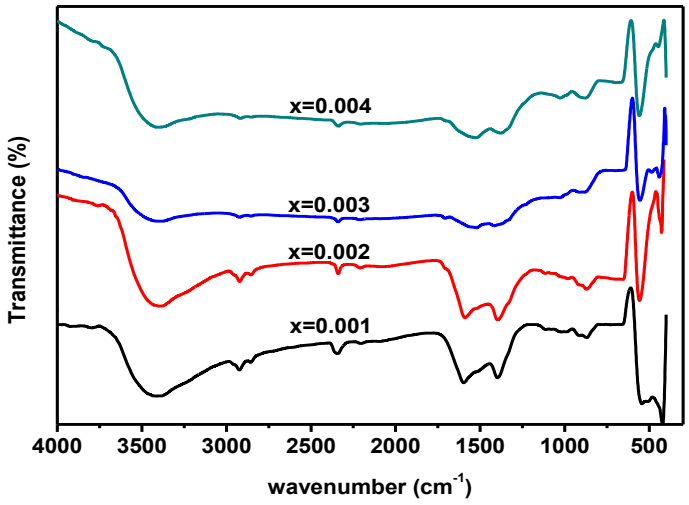

Figure 4 FTIR spectra of $Zn_{1-x}Cu_xO$ nanoparticles

UV-Vis absorption spectrum

The UV-Visible optical absorption spectrum of Cu doped ZnO nanoparticles annealed at 350°C and is shown in **Figure 5a** and Figure 5b. The absorption edge of the sample increases with increasing Cu concentrations indicating that Cu^{2+} ions are incorporated into ZnO lattice. A red shift is exhibited due to the formation of shallow levels inside the band gap by doping and change of electron exchange interactions between the band electrons and the localized d electrons of the Cu^{2+} ion [45].

The optical energy band gap E_g of samples was estimated using the Tauc relation [48],

$$(\alpha h\upsilon) \sim (h\upsilon - E_g)^{1/2}$$

where $h\upsilon$ is the incident photon energy and α is the optical absorption coefficient near the fundamental absorption edge. The absorption coefficients were calculated from the optical absorption spectra. The optical band gap of ZnO was obtained by plotting $(\alpha h\upsilon)^2$ versus $(h\upsilon)$ and the linear region of the plots is extrapolated to $(\alpha h\upsilon)^2 = 0$ as shown in **Figure 6a** and Figure 6b. The estimated band gap energies of Cu doped ZnO nanoparticles are lower than that of pure ZnO (3.37 eV) [45] and are listed in **Table 2**. The band gap increases from 2.59 - 3.159 eV with increase of Cu concentration.

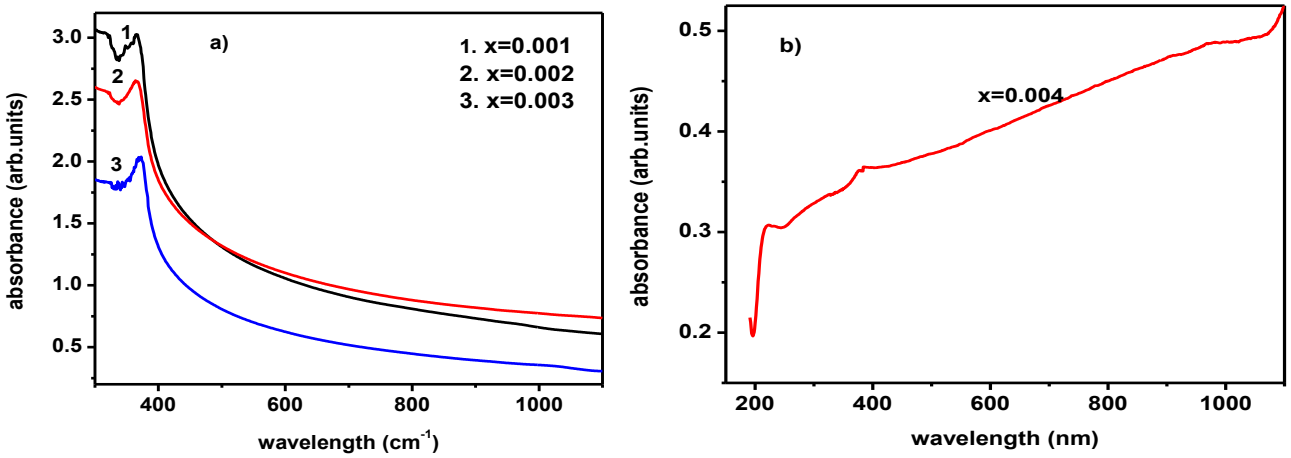

Figure 5 a) and **b)** are optical absorption spectra of $Zn_{1-x}Cu_xO$ nanoparticles

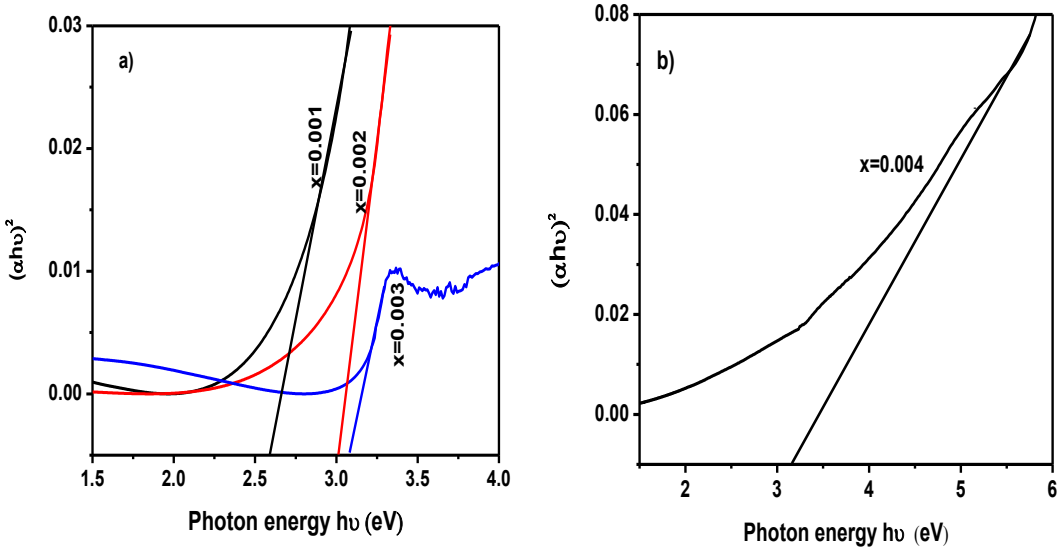

Figure 6 a) and **b)** Band gap energy of $Zn_{1-x}Cu_xO$ nanoparticles

Table 2 Band gap value for $Zn_{1-x}Cu_xO$ nanoparticles

Copper concentration	Band Gap (eV)
x=0.001	2.596
x=0.002	3.013
x=0.003	3.074
x=0.004	3.159

PL studies

PL spectra for Cu doped ZnO nanoparticles annealed at 350°C are shown in **Figure7**. In general, ZnO exhibits one peak near band edge emission (UV region) and one or more defect related emission peaks in the visible region. The visible emission peak of ZnO occurs due to the intrinsic defects such as oxygen vacancies (V_o), Zinc vacancies (V_{zn}), oxygen interstitial (O_i), zinc interstitial (Zn_i), antisite oxygen (O_{zn}) and extrinsic impurities that form deep energy levels in the band gap [49-52]. The PL spectra for our samples show two peaks, a weak intensity peak near 390 nm (3.16 eV) and another strong intensity peak near 607 nm (2.04 eV). The UV emission peak with weak intensity at 3.16 eV is ascribed to the near band edge emission of ZnO which originates from the recombination of free excitons through an exciton – exciton collision process [53-54]. The orange-red emission peak obtained near 607 nm indicates the presence of excess oxygen in the samples such as defects of oxygen interstitials or oxygen vacancies [55- 58]. The defects of oxygen interstitials (oxygen vacancies) represent an oxygen rich (oxygen deficient) state of ZnO. With increasing Cu concentration up to x=0.003, the intensity of the peak gets decreased which may be due to the reduction in the concentration of oxygen vacancies. This in turn decreases the concentration of recombination centre [59-60]. At x=0.004, the intensity of the peak suddenly reaches a high value because of increase in the concentration of oxygen interstitials (oxygen vacancies) and recombination centers.

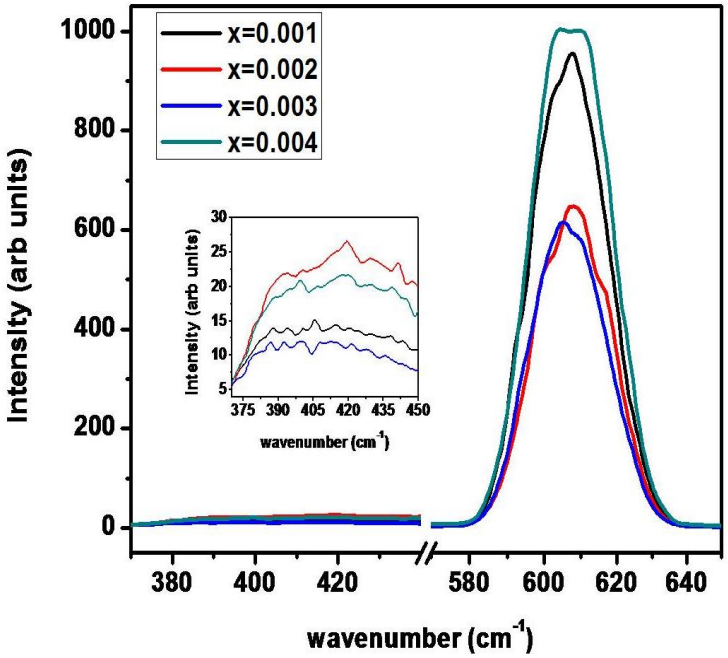

Figure 7 PL emission spectra of $Zn_{1-x}Cu_xO$ nanoparticles.

Conclusions

Cu doped ZnO nanoparticles have been synthesized successfully by solvothermal method. The effect of Cu doping on structural and optical properties was also studied using different characterization techniques. From structural studies based on XRD and TEM, the nanoparticles have a single phase hexagonal structure of ZnO with particle size in the range of 11 - 25 nm. Uniform distribution of nanoparticles has been seen from SEM studies. The elements present in

the samples were recorded using EDX study which confirms the purity of the samples. From FTIR, the functional group of the samples has been identified. The UV-Vis spectrum shows red shifted band edge emission indicating that copper ions are substituted in ZnO lattice sites. A weak intensity near band edge emission peak and a high intensity orange red emission peak were observed in PL spectra. The intensity of orange-red emission peak decreases with increasing concentration up to x=0.003 and this may be due to reduction in the concentration of oxygen vacancies. At higher concentration x=0.004, the intensity of the peak increases suddenly owing to the increasing concentration of oxygen vacancies.

Acknowledgement

The authors are thankful to Managements of The M.D.T. Hindu College, Tirunelveli and Sri Paramakalyani College, Alwarkurichi for their constant and consistent support.

References

[1] Norris D.J., Yao N., Charnock F.T., et al. Nano Letters, 2001, 1, 3.
[2] Feng X., J. Phys.: Condens. Matter, 2004, 16, 4251.
[3] Renzt R., Schulz H.J., J. Phys. C: Solid State Phys., 1983, 16, 4917.
[4] Ohashi N., Ebisawa N., Sekiguchi T., Sakaguchi I., Wada Y., Takenaka T., Haneda H., Appl. Phys. Lett., 2005, 86, 91902.
[5] Ronda C.R., J. Lumin., 1997, 72, 49.
[6] Borgohain K., Mahamuni S., Semicond. Sci. Technol., 1998, 13, 1154.
[7] Meng F., Yin J., Duan Y.Q., Yuan Z.H., Bie L.J., Sensors Actuators B, 2011, 156, 703.
[8] Liu Z., Liu C., Ya J., Lei E., Renew. Energy, 2011, 36, 1177.
[9] Hembram K., Sivaprahasam D., Rao T.N., J. Eur. Ceram. Soc., 2011, 31, 1905.
[10] Kim H., Pique A., Horwitz J.S., Murata H., Kafafi Z.H., Gilmore C.M, Chrisey D.B., Thin Solid Films, 2000, 377, 798.
[11] Barick K.C., Singh S., Aslam M., Bahadur D., Microporous Mesoporous Mater., 2010, 134, 195.
[12] Rekha K., Nirmala M., Nair M.G., Anukaliana A., Physica B, 2010, 405, 3180.
[13] Zhang H., Chen B., Jiang H., Wang C., Wang H., Wang X., Biomaterials, 2011, 32, 1906.
[14] Ozgur U., Alivov Ya.I., Liu C., Teke A., Reshchikov M.A., Dogan S., Avrutin V., Cho S.J., Morko H., J. Appl. Phys., 2005, 98, 041301.
[15] Gorla C.R., Emanetoglu N.W., Liang S., Mayo W.E., Lu Y., M. Wraback M., Shen H., J. Appl. Phys., 1999, 85, 2595.
[16] Xie J., Deng H., Xu Z.Q., Li Y., Huang J., J. Cryst. Growth, 2006, 292, 227.
[17] Janisch R,, Gopal P., Spaldin N.A., J. Phys. Condens. Matter, 2005, 17, 657.
[18] Wolf S.A., Awschalom D.D., Buhrman R.A., Daughton J.M., von Molnar S., Roukes M.L., Chtchelkanova A.Y., Treger D.M., Science, 2001, 294, 1488.
[19] Ding J.J., Chen H.X., Zhao X.G., Ma S.Y., J. Phys. Chem. Solids, 2010, 71, 346.
[20] Ma Z.Q., Zhao W.G., Wang Y., Thin Solid Films, 2007, 515, 8611.
[21] Zhang Z., Yi J.B., Ding J., Wong L.M., Seng H.L., Wang S.J., Tao J.G., Li G.P., Xing G.Z., Sum T.C., Huan C.H.A., Wu T., J. Phys. Chem. C., 2008, 112, 9579.
[22] Zhong J., Muthukumar S., Chen Y., Lu Y., Appl. Phys. Lett., 2003, 83, 3401.
[23] Yamada T., Miyake A., Kishimoto S., Makino H., Yamamoto N., Yamamoto T., Surf. Coat. Tachnol., 2007, 202, 973.
[24] Tao Y.M., Ma S.Y., Chen H.X., Meng J.X., Hou L.L., Jia Y.F., Shang X.R., Vacuum, 2011, 85, 744.
[25] Niasari M.S., Davar F., Khansari A., J. Alloys Compd., 2011, 509, 61.
[26] Yang J., Feia L., Liua H., Liu Y., Gaoa M., Zhanga Y., Yanga L., J. Alloys Comp., 2011, 509, 3672.
[27] Yang Y., Chen H., Zhao B., Bao X., J. Cryst. Growth, 2004, 264, 447.
[28] Hu J.Q., Li Q., Wong N.B., Lee C.S., Lee S.T., Chem. Mater., 2002, 14, 1216.
[29] Lao J.Y., Huang J.Y., Wang D.Z., Ren Z.F., Nano Lett., 2003, 3, 235.
[30] Chauhan R., Kumar A., Chaudharya R.P., J. Chem. Pharm. Res. 2010, 2, 178.

[31] Savu R., Parra R., Joanni E., Jancar B., Elizario S.A., de Camargo R., Bueno P.R., Varela J.A., Longo E., Zaghate M.A., J. Cryst. Growth, 2009, 311, 4102.
[32] Elilarassi R., Chandrasekaran G., Optoelectron. Lett., 2010, 6, 6.
[33] Suwanboon S., Amornpitoksuk P., Bangrak P., Ceram. Int. 2011, 37, 333.
[34] Rao K.J., Vaidhyanayhan B., Ganguli M., Ramakrishnan P.A., Chem. Mater., 1999, 11, 82.
[35] Liao X.H., Zhu J.M., Xu J.Z., Chen H.Y., Chem. Commun., 2001, 937.
[36] Liang J., Deng Z., Jiang X., Li F., Li Y., Inorg. Chem., 2002, 41, 3602.
[37] Wang H., Xu J.Z., Zhu J.J., Chen H.Y., J. Cryst. Growth, 2002, 224, 88.
[38] Gallis K.W., Landry C.C., Adv. Mater., 2001, 13, 23.
[39] Palchik O., Zhu J., Gedanken A., J. Mater. Chem., 2000, 10, 1251.
[40] Boxall D.L., Lukehart C.M., Chem. Mater., 2001, 13, 806.
[41] Varadhaseshan R. Meenakshi Sundar S., Applied Surface Science, 2012, 258, 7161.
[42] Gandhi V., Ganesan R., Abdukrahman Syedahamed H.H., Mahalingam T., J. Phys. Chem C., 2014, 118, 9715.
[43] Singhal S., Kaur J., Namgyal T., Sharma R., Physica B., 2012, 407, 1223
[44] Muthukumaran S., Gopalakrishnan R., Opt. Mater., 2012, 34, 1946.
[45] Reddy A.J., Kokila M.K., Nagabhushana H., Chakradhar R.P.S., Shivakumara C., Rao J.L., Nagabhushana B.M., J. Alloys Compd., 2011, 509, 5349.
[46] O. Perales-perez, A. Parra-Palomino, R. Singhal, P.M. Voyles, Y. Zhu, W. Jia, M.S. Tomar Nanotechnology, 2007, 18, 315606.
[47] Elilarassi R., Chandrasekaran G., Amer. J. Mater. Sci., 2012, 2, 46.
[48] Nagabhushana H., Nagabhushana B.M., Madesh Kumar, Premkumar H.B., Shivakumara C., Chakradhar R.P.S., Philos. Mag. 2010, 26, 3567.
[49] Vanheusden K., Seager C.H., Warren W.L., Tallent D.R., Voigt J.A., Appl. Phys. Lett., 1996, 68, 403.
[50] Xu P.S., Sun Y.M., Shi C.S., Xu F.Q., Pan H.B., Nucl. Instrum. Methods Phys. Res., Sect. A, 2003, 199, 286.
[51] Bylander E.G., Appl. Phys., 1978, 49, 1188.
[52] Liu M., kitai A.H., Mascher P., J. Lumin., 1992, 54, 35.
[53] Elilarassi R., Chandrasekaran G., Mater. Chem. Phys., 2010, 123, 450.
[54] Shinde K.P., Pawar R.C., Sinha B.B., Kim H.S., Oh S.S, Chung K.C., Ceram. Int., 2014, 40, 16799.
[55] Tam K.H., Cheung C.K., Leung Y.H., Djurisic A.B., Ling C.C,, Beling C.D., Fung S., Kwok W.M., Chan W.K., Phillips D.L., Ding L., Ge W.K.., J. Phys. Chem. B, 2006, 110, 20865
[56] Wu X.L, Siu G.G., Fu C.L., Ong H.C., Appl. Phys. Lett., 2001, 78, 2285.
[57] Panigrahy B., Aslam M., Misra D.S., Ghosh M., Bahadur D., Adv. Func. Mater., 2010, 20, 1161.
[58] Qiu J., Li X., Zhuge F., Gao X., He W., Park S.J., Kim H.K., Hwang Y.H., Nanotechnology, 2010, 21, 195602.
[59] Wang M., Cheng X., J. Yang, Appl. Phys. A, 2009, 96, 783.
[60] Yilmaz S., McGlynn E., Bacaksiz E., Cullen J., Chellapan R.K., Chem. Phys. Lett., 2012, 525, 72.

Publication History

Received	15th	Apr	2016
Accepted	05th	May	2016
Online	30th	Jun	2016